# Solvent Tuning of a Conical Intersection: Direct Experimental Verification of a Theoretical Prediction

**ARTICLE** *in* THE JOURNAL OF PHYSICAL CHEMISTRY A · AUGUST 2011

Impact Factor: 2.69 · DOI: 10.1021/jp206412h · Source: PubMed



**5 AUTHORS**, INCLUDING:

Anat Kahan
Hebrew University of Jerusalem
**11** PUBLICATIONS **101** CITATIONS
SEE PROFILE

Amir Wand
Hebrew University of Jerusalem
**16** PUBLICATIONS **125** CITATIONS
SEE PROFILE

Shmuel Zilberg
Ariel University
**66** PUBLICATIONS **1,122** CITATIONS
SEE PROFILE

Yehuda Haas
Hebrew University of Jerusalem
**66** PUBLICATIONS **1,206** CITATIONS
SEE PROFILE

THE JOURNAL OF PHYSICAL CHEMISTRY A

ARTICLE

pubs.acs.org/JPCA

# Solvent Tuning of a Conical Intersection: Direct Experimental Verification of a Theoretical Prediction

Anat Kahan,[†] Amir Wand,[†] Sanford Ruhman,* Shmuel Zilberg, and Yehuda Haas*

Institute of Chemistry and the Farkas Center for Light-Induced Processes, The Hebrew University of Jerusalem, Jerusalem 91904, Israel

Supporting Information

**ABSTRACT:** We report an ultrafast study of a merocyanine molecule, whose fluorescence lifetime was tuned by changing the solvent's polarity. A recent theoretical prediction that the fluorescence lifetime is considerably shortened upon lowering the polarity of the solvent, due to tuning of the conical intersection properties, is fully confirmed (Xu et al. *J. Phys. Chem. A* **2009**, *113*, 9779−9791). This constitutes a direct measurement of a previously predicted tunable property of a conical intersection.

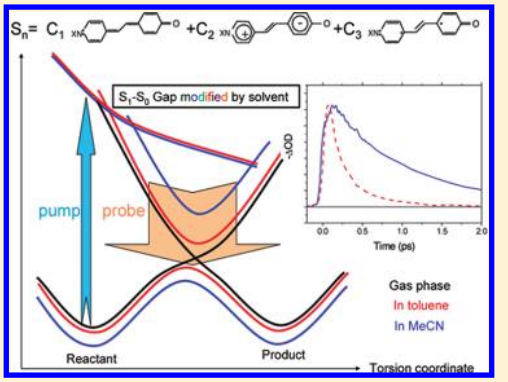


## A. INTRODUCTION

Conical intersections (CIs) are now believed to be important factors in the photochemistry of polyatomic molecules.[1−4] Their properties have been mainly explored computationally, using quantum chemical methods. The ultra-short-lived electronically excited states in many photoreactive systems, the concomitant reduction in their fluorescence quantum yields, along with the ultrafast production of products, have all been attributed by theoretical modeling to the existence of CIs connecting excited and ground electronic surfaces.[4−8] In a recent example, ultrafast work on the bovine visual pigment Rhodopsin tracked coherent wavepacket motion from the photoexcited Franck−Condon (FC) region to the photoproduct of the reaction, showing good agreement to molecular dynamics simulations, based on the existence of a conical intersection.[9] Farrow et al. have used polarized femtosecond pump−probe spectroscopy to observe electronic wavepacket motion for vibrational wavepackets centered on a CI.[10]

Being of such fundamental importance in photochemistry, controlling the properties of CIs and the transitions through them has been the subject of numerous studies. A particularly convincing proof of their existence and dynamic significance would be identification of a physical variable that can be tuned continuously, and shown to directly affect a CI. A few methods of CI tuning have been suggested, relying on the basic concept of controlling the reaction pathways and excited state dynamics of chemical reactions.[11] These include modification of the potential energy surfaces (PES), either by environmental effects[12−14] or application of external fields.[15,16] Alternatively, dynamics at the CI could be controlled by custom-tailoring of the excited nuclear wavepacket.[17] A recent work has combined both approaches by suggesting manipulating the trajectory of the nuclear wavepacket by modifying the PES using substitution of functional groups in a molecule, in a so-called "intramolecular orbital alignment".[18]

Of particular interest here are the effects of solvation and of electric fields on the properties of CIs. Hynes, Burghardt, and co-workers examined theoretically the effect of solvent polarity on conical intersections.[13] Improta and co-workers experimentally investigated how shifting between polar solvents altered photochemistry of various DNA bases and their derivatives.[19] Solvent effects were also studied experimentally by Briand et al. for a *cis*−*trans* isomerization reaction in an artificial molecular switch in methanol.[20] Takatsuka and co-workers theoretically demonstrated an approach of CI tuning using a control pulse, as a means of symmetry-breaking, capable of "converting" a CI to an avoided-crossing. This was explained in terms of modulating the PES to move the geometry of the original CI.[21] The effect of a strong electromagnetic field was studied experimentally in the gas phase by Sussman et al., who employed a strong IR laser field to induce a dynamic Stark effect to modify the dissociation dynamics of IBr. In this case, a conical intersection is not involved, but the experiment highlights the ability of electric fields in the gas phase to modify the potential energy surface.[16]

Striving to achieve similar CI tuning, Xu et al. demonstrated theoretically that in some merocyanine molecules, a strong electric field can be used to modify or even eliminate the CI between the two lowest potential surfaces.[22] In principle, these changes can be observed experimentally by monitoring the fluorescence lifetime as a function of an applied DC field. However, the required fields are prohibitively high, rendering this approach

**Received:** July 7, 2011
**Revised:** August 19, 2011
**Published:** August 22, 2011

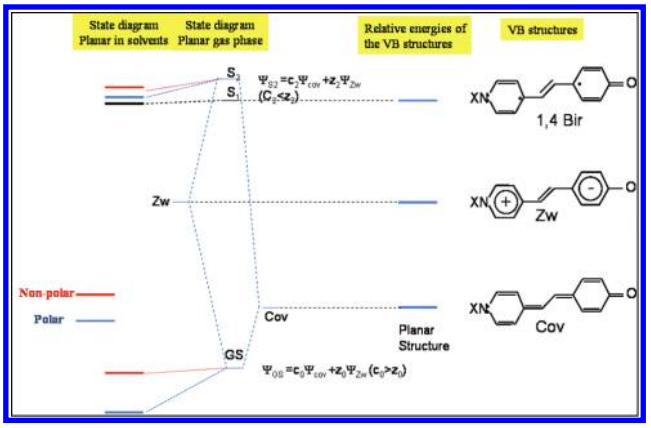


**Figure 1.** Scheme showing the construction of the three lowest singlet states of mrcn from 3 basic VB structures, based on ref 22. The contribution of the biradical VB form to the GS and $S_2$ is negligible. On the left-hand side, the solvent effect on the planar molecule in the FC region is shown. The $S_2$ state is more polar that the GS, so that in polar solvents the GS, that becomes more polar, undergoes a greater stabilization than the excited state, whose structure is not changed much, and a blue shift is observed. In nonpolar solvents, the stabilization of both GS and $S_2$ is smaller than in polar solvents. However, stabilization of $S_2$ is larger as it is due to the ZW part, and a smaller blue shift results.

impractical in liquid solution. To overcome this, one can alternatively change the solvent's polarity, which was shown in the same work to be equivalent to varying the electric field. The effect of solvent on dynamics in the singlet manifold was discussed using terms of three VB structures: one covalent (Cov), the second charge-separated (ZW), and the third biradical ($Bir_{14}$).[22] Figure 1 presents the resulting energy level diagram of the three low-lying singlet states, which are described as linear combinations of the three VB structures. The biradical VB structure has a very small contribution, which may be neglected, to the GS and also to $S_2$, while $S_1$ is mainly of biradical nature. When inserted into a solvent, the electronic states and corresponding energies undergo polarity-dependent shifts, again mainly affecting GS and $S_2$, but not $S_1$. In the gas phase, the contribution of the ZW structure to $S_2$ is larger than to the GS. However, polar solvents, having a local effect of electric field, change the relative contribution of the two VB structures, so that the GS becomes more ionic. Stabilization of the GS is larger than that of $S_2$, which is already mostly polar (large ZW contribution) even in the gas phase, usually leading to a blue shift. The small polarity of the nonpolar solvent affects the $S_2$ state more than the GS and a red shift arises (see also, ref 23 and 24). It was also predicted that in the case of "Push−Pull" molecules such as merocyanines, the $S_1-S_0$ energy gap for the relaxation process is considerably increased in a polar solvent compared to a nonpolar one, leading to a longer excited state lifetime in the former.

That prediction is tested in the current study. The molecule studied is shown in Figure 2. Merocyanines are readily soluble in polar solvents. In order to facilitate dissolution in liquids of varying polarity, two tert-butyl moieties were used as substituents (sites $R_2$ and $R_3$ in the Figure). The molecule will hitherto be coined di-tBu-mrcn. The di-tBu-mrcn molecule was dissolved in dry toluene ("non-polar") and dry acetonitrile ("polar"), both of which are aprotic solvents. The solvatochromic properties of the family of merocyanines were studied thoroughly, and are discussed later in the context of this specific derivative.[25,26]

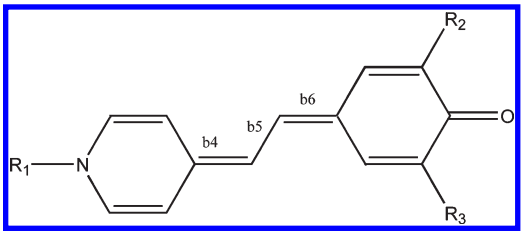


**Figure 2.** Merocyanine-derivative molecule (di-*t*Bu-mrcn) used in the experiments, $R_1$=$CH_3$. $R_2$=$R_3$=*t*Bu. The two *tert*-butyl moieties are present to facilitate solution in nonpolar solvents.

Experimentally, the predicted effect can be observed either in time-domain measurements (longer lifetime of the excited state population) or in steady-state frequency-domain measurements (stronger emission) in polar solvents relative to nonpolar solvents. Regarding the former, previous ultrafast studies of merocyanines or similar molecules[27−29] have revealed alterations in lifetimes or quantum yields of fluorescence with variation of solvent polarity. These works were generally interpreted in terms of locally excited versus charge transfer states in the solvents, not dealing with the possibility of tuning the conical intersections involved in the process.

In this work, we report a direct measurement of the fluorescence lifetime of a merocyanine derivative using ultrafast pump−probe spectroscopy (<100 fs resolution). In line with the theoretical predictions, also augmented by steady state measurements presented here, the observed lifetime in acetonitrile (MeCN) is ∼2−3 times longer than in toluene. This constitutes direct experimental evidence for a conical intersection being tuned by a previously calculated environmental effect.

## B. EXPERIMENTAL SECTION

The di-*t*Bu-mrcn molecule was prepared according to literature procedures.[30,31] Me-mrcn ($R_1$=$CH_3$, $R_2$=$R_3$=H in Figure 2) was purchased from Sigma-Aldrich. Dry powders, dried over $P_2O_5$ in vacuum, were kept in the dark. To avoid protonation in solution,[32] the di-*t*Bu-mrcn molecule was dissolved in dry toluene and acetonitrile, used as received. Other solvents used for absorption measurements were of spectroscopic grade. The solutions were saturated with nitrogen to avoid oxidation and kept in the dark prior to experiments.

**B.1. Steady State Measurements.** Absorption spectra were recorded using an HP8425 spectrophotometer. Steady state fluorescence measurements were obtained using a Cary Eclipse fluorimeter (Varian), with a 10 nm excitation and emission slit widths. The sample's OD at the absorption peak was typically 0.2−0.3, slightly high, in order to improve the S/N ratio of the low quantum yield fluorescence. Because this might lead to self-absorption at the red edge of the absorption spectra, the obtained quantum yields (QYs) were checked by integration of the spectra over different domains. The measured fluorescence spectra were corrected for the instrumental response using a Cresyl Violet emission spectrum, that was also used as reference for quantum yields (QYs) calculation (QY = 0.578 in ethanol).[33] Since this correction procedure becomes very sensitive for $\lambda$ > 750 nm under the conditions, the corrected spectra are shown in what follows only for shorter wavelengths.

**B.2. Ultrafast Measurements.** The ultrafast experimental system was described in detail previously.[34] Briefly, laser pulses of ∼30 fs duration and centered at 790 nm (∼0.5 mJ/pulse)

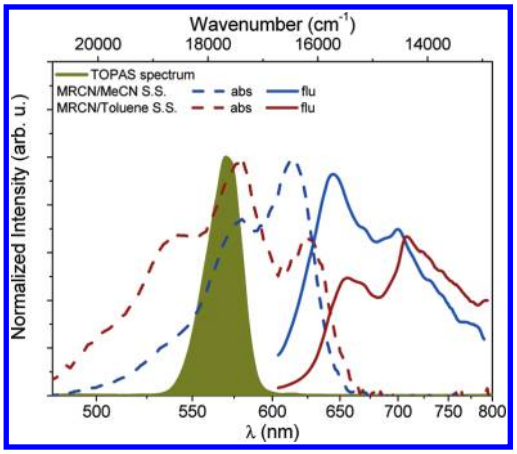


**Figure 3.** Steady state absorption spectra (dashed lines) and corrected fluorescence spectra (after excitation at 580 nm, shown in solid lines) of di-*t*Bu-mrcn (see Figure 2) in MeCN (blue) and toluene (red), shown along a typical excitation spectrum produced by the TOPAS and used in the ultrafast experiments. The data are normalized and shown on an arbitrary unit scale, with the fluorescence data preserving the measured experimental ratio of amplitudes and scaled to preserve the photon flux density in the wavenumber space ($F(\bar{\nu})/(\bar{\nu}^2)$).

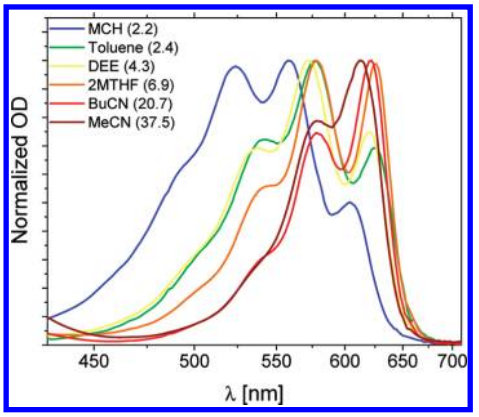


**Figure 4.** UV−vis steady-state absorption spectra of di-*t*Bu-mrcn in a series of aprotic solvents covering a range of polarity (designated in legend). Abbreviations used (from nonpolar to most polar): methylcyclohexane (MCH), toluene, diethyl ether (DEE), chloroform ($CHCl_3$), 2-methyl-tetrahydrofuran (2MTHF), butyronitrile (BuCN), acetone, MeCN, and dimethylsulfoxide (DMSO). The numbers in parentheses are the dielectric constants of the solvents.

were derived from a homemade multipass Ti:Sapphire amplifier, operated at 400 Hz. 50% of the output was used to pump a parametric amplifier (TOPAS, Light Conversion), generating ~30 fs pulses centered at 570 nm, which were used as the pump pulses (whose spectrum is depicted in Figure 3). Probing was conducted with multifilament supercontinuum radiation, generated by focusing part of the remaining fundamental into 2.5 mm of Sapphire. The continuum pulses were split into probe and reference pulses, collected later by fibers into a double spectrometer setup, allowing multichannel generation of time-dependent difference spectra in the range from 500 to 900 nm. Pump chirp was compensated by a prism pair, leading to compression to ~40 fs. ΔOD maps were corrected for the measured group delay dispersion (GDD) of the probe continuum by interpolation and temporal reshuffling of the different spectral cuts.

## C. RESULTS

**C.1. Steady State Measurements.** The UV−vis absorption spectra of di-*t*Bu-mrcn in MeCN and toluene are shown in Figure 3, along with the corresponding room-temperature steady state fluorescence spectra. The most noticeable features in the absorption spectra are a broader progression of vibronic peaks in toluene solution relative to that in MeCN, accompanied with a negligible shift of the 0−0 transition frequency. We conclude that in less polar solvents the degree of structural rearrangement involved in the electronic transition is enhanced, leading to larger vibronic displacements and vibrational rearrangement energies. This leads to the more extended high frequency mode vibronic progression in toluene relative to that observed in acetonitrile (see Introduction and Figure 1). To further check this, Figure 4 presents the UV−vis absorption spectra of di-*t*Bu-mrcn in a series of aprotic solvents, covering a wide range of polarities. As seen in the figure, the main effect of solvent polarity on the di-*t*Bu-mrcn absorption spectrum is due to geometry changes rather than the tuning of the 0−0 transition. These geometric changes are directly related to the vertical excitation energies, allowing for experimental verification of our previous theoretical study results (see Figure 5 in ref 22), in which it was concluded that as the electric field (polarity) is *increased*, the vertical excitation energy is *decreased*. This rule also applies for the extensively studied Brooker's merocyanine in solvents with different polarities.[37] However, comparing to the latter, the absorption spectra of the di-*t*Bu derivative are much more vibronically structured.

This interpretation of the differences in the steady state spectra in terms of geometric displacements is expected to have direct influence on the primary dynamics following photoexcitation, as the driving force on the excited state is expected to be larger in toluene than in MeCN.

Figure 3 also shows corrected emission spectra of di-*t*Bu-mrcn in toluene and MeCN. The different excitation wavelengths that were used (in the range of 570−600 nm) gave the same line shapes and QYs. The measured QYs were $(3.5 \pm 0.5) \times 10^{-4}$ and $(1.3 \pm 0.1) \times 10^{-4}$ for MeCN and toluene, respectively. Using these QYs, the fluorescence lifetimes were calculated from the Strickler−Berg equation,[35] to be 1200 ± 200 fs in MeCN and 380 ± 40 fs in toluene.

**C.2. Femtosecond Spectroscopy.** Figure 5 presents the time-corrected transient difference absorption spectra for di-tBu-mrcn in both solvents (MeCN in the left-hand side and toluene in the right-hand side). The data are presented in upper panels as color-coded contour maps of ΔOD as a function of delay and probe wavelength, with an extended scale up to 2 ps. The lower panels present sequences of temporal cuts in those maps at designated time delays. The steady-state absorption and corrected fluorescence spectra were added to the middle panels in dashed and dotted black lines, respectively. All maps and cuts are shown on the same scale for comparison.

In both solvents, immediately following photoabsorption, a bleaching of ground state absorption is observed at the blue end of the probed spectrum, accompanied by characteristic vibronic progressions. This increased transmission, however, spreads further to the red compared to the ground state absorption due to contributions from excited state stimulated emission. The emission also evolves spectrally, both red-shifting and spreading with time. These features decay on a few picoseconds time scale, leaving behind hot ground state populations which cool down on a time scale of tens of picoseconds. This appears as an excess

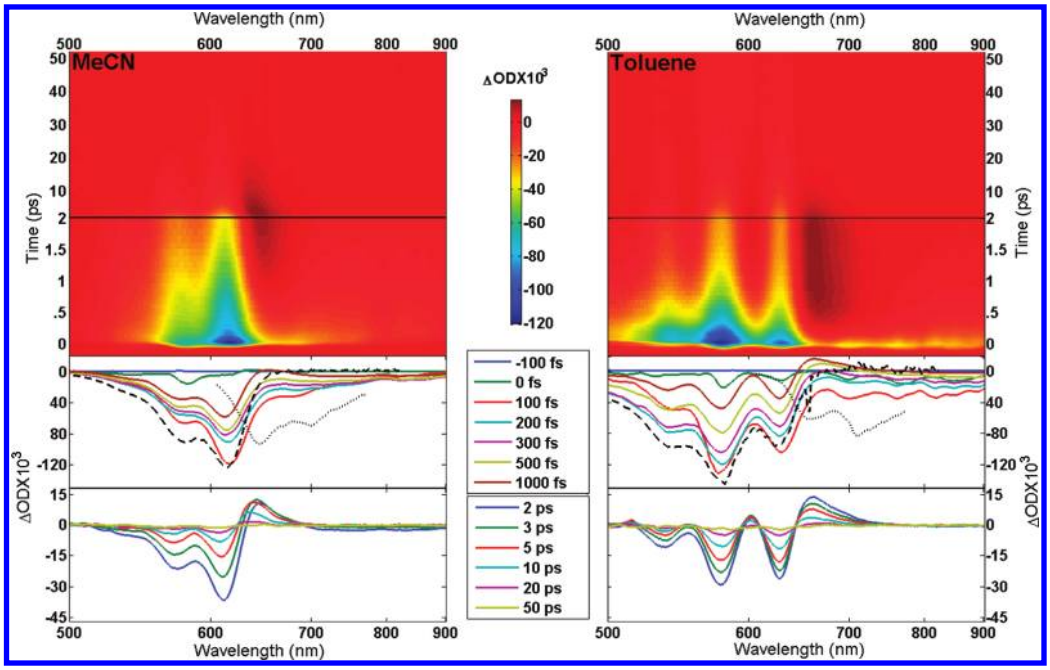


**Figure 5.** Transient difference absorption spectra of di-*t*Bu-mrcn in MeCN (left panel) and in toluene (right panel), corrected for probe group delay dispersion. The upper panels present the data as a contour map from −0.2 to 50 ps, with an expanded scale up to 2 ps. The two lower panels depict temporal cuts of the same data at the designated pump−probe delays, with the middle one corresponding to short delays, and the lower one corresponding to longer delays. The steady state absorption and fluorescence spectra at each solvent are depicted in the middle panel, superimposed on the transient cuts, in black dashed and dotted lines, respectively, as a handy reference (fluorescence spectra were corrected as described in the text).

absorption ($\Delta OD > 0$) in the red part of the steady state absorption spectrum (around 650−700 nm), and as additional peaks around 550 and 600 nm in the case of toluene only. These features, which are due to overpopulation of high-states in the ground state vibrational ladder, gradually diminish in amplitude, as the molecule relaxes to room temperature. Spectral cuts at designated wavelengths are shown in Figure 6 with each panel depicting the corresponding cut for MeCN (blue lines) and toluene (red lines). The cuts are shown at wavelengths dominated by excited state emission ($\lambda_{pr} > 600$ nm), which provide a more reliable measure of excited state lifetimes that are observably shorter in toluene than in MeCN.

**C.3. Kinetic Analysis.** To quantify these differences, a sequential kinetic model of the form

$$A^* \xrightarrow{1/\tau_1} B^* \xrightarrow{1/\tau_2} A_H \xrightarrow{1/\tau_3} A$$

was applied, with A being the ground state reactant, and A*, B*, and $A_H$ being species created after photoexciation, on the way to recovery of the relaxed ground state. The (time-corrected) data were analyzed using Singular Value Decomposition (SVD), followed by a global fit to the above scheme.[36] This yields Species Associated Difference Spectra (SADS). Each component was convoluted with a Gaussian Instrumental Response Function (IRF) of ∼80 fs (fwhm). In view of the large amplitude of the ground state bleach on the blue end of our spectral range, global fitting was conducted iteratively. A preliminary run concentrated on the red part of the probe spectrum which is dominated by excited state activity. In both solvents, these data were well-fit with two exponential decay components, with lifetimes of $\tau_1$ = 90 ± 20 fs and $\tau_2$ = 890 ± 70 fs in MeCN and $\tau_1$ = 80 ± 20 fs and $\tau_2$ = 350 ± 40 fs in toluene. Having performed this reduced global fitting, the obtained lifetimes were used as an initial guess for a global fit of the entire transient spectral data. In that case, a three-step kinetic model was found to provide a satisfactory fit. Figure 7 presents the results of the global analysis of the entire transient spectral data using the three-step model involving three species A*, B*, and $A_H$ (representing hot ground state, see also Discussion). The figure shows the SADS characterizing these species, along with the obtained associated time constants, for both data sets. Lifetimes for the first two steps agree with those obtained in the preliminary reduced fit, justifying the iterative approach of target analysis.

## D. DISCUSSION

In this section, the reported results are interpreted in terms of the theoretical treatment presented in ref 22. This is performed despite the effects of the di-*t*Bu substitution on the absorption spectra, since the basic energy level diagram of the merocyanine is not changed by substitution. The same three VB structures are believed to be playing key roles in defining the nature of electronic states involved, with the substitution only masking solvation sites of the chromophore as described below.

**D.1. Steady State Absorption Spectra and Solvent Effects.** The steady-state absorption spectra of di-*t*Bu-mrcn in a range of solvents (see Figure 4) are dominated by a vibrational progression, assigned to the totally symmetric C═C normal mode of the chain in the excited state (∼1600 $cm^{-1}$), with an additional contribution of the 1280 $cm^{-1}$ mode in the polar solvent spectrum. In contrast, in the case of Me-mrcn, the vibronic features are washed out in polar solvents.[37] The attached *t*-Bu groups in di-*t*Bu-mrcn appear to have at least a 2-fold effect: first, the solvent effects might be masked by the bulky *t*-butyl groups, as suggested by Catalan et al.;[37] second, the electron donating character of the butyl moieties tends to increase of the electron

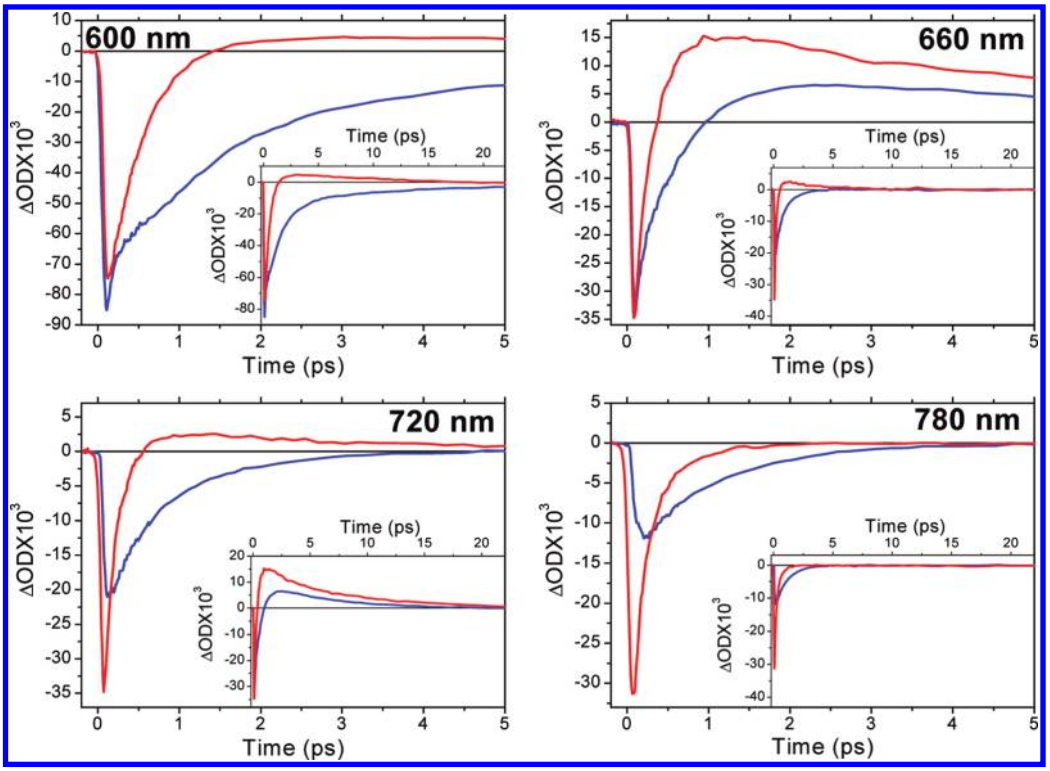


**Figure 6.** Spectral cuts of pump−probe data of di-*t*Bu-mrcn (Figure 5) at few wavelengths in the red portion of probing (specific wavelengths designated inside panels). The data for solvation in MeCN is shown in blue lines and for toluene in red lines, clearly demonstrating a faster excited state decay of the latter. The main panels depict the short-time traces (up to 5 ps), while the insets show the long-time behavior (up to ∼20 ps).

density on the keto-cyclohexadienyl moiety, reducing its electron drawing strength. At present, quantitative measures of these effects are not available. Moreover, to exclude the possibility that the structure observed is due to multiple conformations and aggregates, as was suggested for similar dyes,[38] these spectra were shown to be unchanged upon dilution by a factor of 10 or more. In addition, it has been recently suggested that self-aggregation is not likely to occur in nonpolar solvents.[39]

Having assigned this structure to vibronic progressions, the broader and more pronounced structure in toluene is interpreted to be the result of a larger relative structural change between the ground and excited state PESs in the nonpolar solvent. It is in accord with the model wherein the GS is mainly covalent in these solvents, whereas it becomes mostly ZW in polar solvents becoming more similar to $S_1$, the excited ZW twin state. The steady state absorption spectra are, therefore, in line with the higher vibrational reorganization energy in toluene relative to that in MeCN.

In light of the prevailing explanation of solvatochromism in merocyanines in terms of stabilization of the electronic states, we note that a recent work by Mustroph et al. offers similar observations to ours.[40] Based on calculations and absorption spectra of a different mrcn derivative, they too conclude that the solvents affect the absorption mainly by varying the degree of vibrational reorganization rather than by shifting the 0−0 energy gap. This is supported by calculations and NMR measurements, which show that when moving to polar solvents, the bond-length alternation (BLA) in the conjugated chain decreases, which leads to smaller shifts of $R_{eq}$ between the two lowest PESs.

To further quantify the observed vibronic broadening, the absorption spectra of di-*t*Bu-mrcn in both solvents were reconstructed using the simplest (DHO) of displaced harmonic oscillator model based on Heller's formalism.[41] The details of this analysis can be found in the Supporting Information. Briefly, the absorption spectra were well-reproduced by changing the displacement of the 1600 $cm^{-1}$ mode from $\Delta = 0.35$ to $\Delta = 0.85$ for MeCN and toluene, respectively, while nearly conserving the 0−0 transition energy. These values are physically reasonable for such molecules, lending further support to our explanation. The oscillator strength of the allowed transition contributing to the absorption band was calculated using the DHO fit to be 1.9 in toluene and 1.6 in MeCN. These values are compatible with the calculations (1.5 in toluene and 1.4 in MeCN) and with literature estimates.[22,42−44]

**D.2. Steady State Fluorescence.** Within limitations of our fluorimeter's spectral range, the corrected fluorescence and absorption spectra exhibit a vibronic structure that roughly approximates a mirror image, with a ∼780 $cm^{-1}$ Stokes shift in both solvents, as depicted in Figure 3. Because the existence of mirror image suggests that the fluorescence arises from the same state to which population is promoted directly by absorption from the GS, we conclude that in both solvents the lowest lying excited singlet state in the Franck−Condon region, and the state to which population is promoted by absorption, is primarily ZW and not biradical in nature. This state is the anticombination of the same two VB structures, which create the ground state (Figure 1) and, thus, this transition is optically allowed.

The measured fluorescence QYs of $(3.5 \pm 0.5) \times 10^{-4}$ in MeCN and $(1.3 \pm 0.1) \times 10^{-4}$ in toluene, are both of the same order of magnitude as in previous measurements[37] The natural lifetime of the molecule in these solvents is, thus, about 3 ns, as estimated by Strickler−Berg equation. Using the expression $QY = \tau_m/\tau_{rad}$, where $\tau_m$ and $\tau_{rad}$ are the measured and the

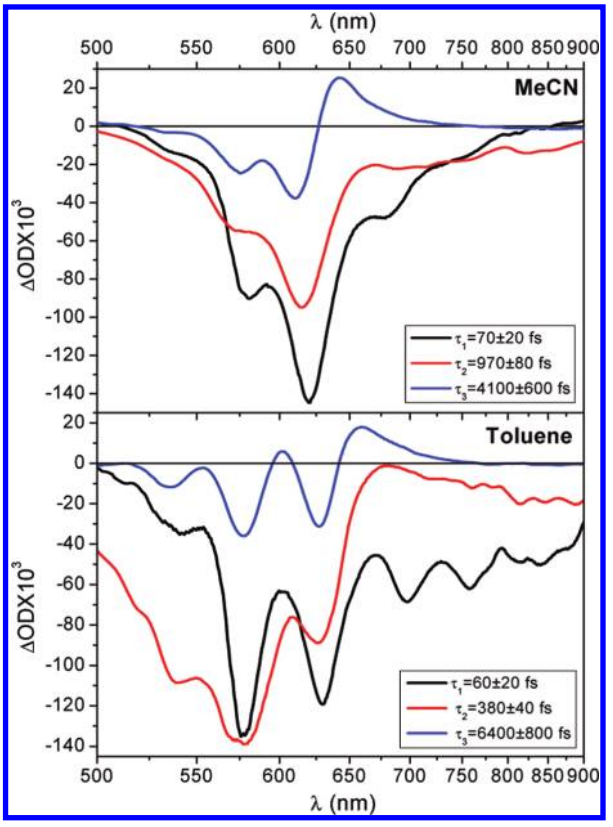


**Figure 7.** Species Associated Difference Spectra (SADS) derived by global fitting of the time-corrected data of the entire transient spectral data (Figure 5) to a three-step sequential kinetic scheme, convoluted with a Gaussian IRF of ~80 fs fwhm. The obtained time constants for each species are depicted. The upper panel corresponds to the MeCN data, while the lower panel to the toluene data.

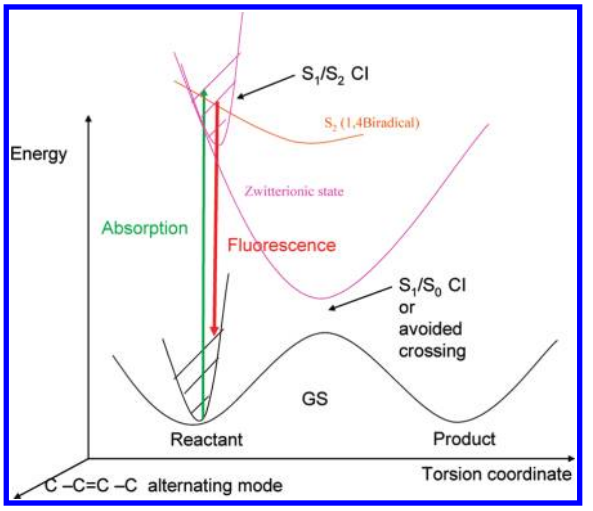


**Figure 8.** Schematic energy level diagram (based on ref 22) for di-*t*Bu-mrcn in a solvent, shown along the two coordinates associated with the $S_0/S_1$ CI: symmetrical stretching and torsion (see text for details). The energy ordering of states in the FC region might differ, as explained in text.

radiative lifetimes, respectively, we find that the difference between the measured lifetimes in toluene and MeCN is in line with the trend found in the theoretical work.[22] The absolute values of the $\tau_m$s also agree with those extracted from the femtosecond experiments, within the estimated experimental error.

**D.3. Ultrafast Measurements and the Kinetic Model.** A three-step sequential kinetic model was shown above to provide a satisfactory fit to the reported ultrafast data (section C.3). Assignment of the species responsible for the three steps will be conducted using an energy level diagram of di-*t*Bu-mrcn in solvents (shown in Figure 8), based on our previous theoretical work[22] and on the present experimental data. The calculations (ref 22) found that whereas in the gas phase the biradical state lies 0.35 eV lower than the ZW state, in the solvents the gap is narrowed to about 0.17 eV. Such a small difference is beyond the real accuracy of the CASSCF method, and for the reasons cited above identification of the $S_1$ as ZW in nature is deemed more compatible with the experimental observations and adopted herein. In view of the mirror-image relationship found between the absorption and emission spectra in both solvents, we assume that the ZW state is $S_1$ in these solvents. The two coordinates depicted define the $S_0/S_1$ conical intersection. From the SS absorption vibronic progression, it is clear that the C═C stretch (mainly a C═C−C═C ↔ C−C═C−C alternating mode) to which the 1600−1700 $cm^{-1}$ band is assigned, is a dominant motion on the way to the $S_1/S_0$ conical intersection. Together with this motion, the second coordinate needed to reach the geometry of the conical intersection is the torsion around a C═C bond, as the geometry at the minimum of the ZW state is perpendicular whereas in the FC region it is planar. These two coordinates are commonly employed in interpretation of IC of systems with *cis*−*trans* photoisomerization

Given the briefness of primary events observed in the toluene solutions, a zero order assignment for the model species ($A^*$, $B^*$, $A_H$) will be based on analysis of results in acetonitrile, later to be transferred by analogy to the toluene data as well. Accordingly, initial excitation is to the allowed ZW state, which is $S_1$ in the FC region. The first step in both solvents is dominated by bleach and stimulated emission signals, with the latter still preserving a strong vibrational progression to be washed out at later times. The time constants of this step (step 1) are similar in both solvents but are also very close to our experimental temporal resolution. Based on the rough mirror image of absorption and steady state emission spectra and the agreement of lifetimes associated with the *second* kinetic stage with Strickler−Berg estimates of the lifetimes of the fluorescent states, we assign the first process to nuclear reorganization in the excited state, possibly including solvent reorganization as well. Similar stages of spectral evolution have been reported in other ultrafast spectroscopic studies of conjugated hydrocarbons such as retinal derivatives, and specifically associated with vibrational reorganization along the carbon backbone heralded by vibronic progressions such as those described above. Due to the marginal time resolution, this feature may also have contributions from coherent coupling of the overlapping pump and probe. This first kinetic phase is assigned similar lifetimes in both solvents, possibly indicating that the pulses used are insufficiently short to resolve this step. It is noteworthy that in any case, this initial stage should be "dynamic" and not "kinetic" in nature, characterized by continuous spectral evolution, and bound to be relatively unsatisfactorily described by a kinetic model.

Following the first step, the $S_1$ (ZW) state proceeds to the CI with $S_0$. The spectrum of the second species ($B^*$) obtained in analysis of the acetonitrile data consists of continuing ground

state bleach, along with a less structured and shallow emission. The time constants of this step are similar to those obtained in the reduced global fitting procedure, supporting its assignment to excited state decay. We therefore assign species B* to the ZW ($S_1$) state, and the second stage of spectral evolution, to internal conversion from $S_1$ to the ground state (see also panel A of Figure S2 in the Supporting Information). As shown in ref 22, the minimum gap between the two states is smaller in the nonpolar solvent than in the polar one (Figures 9 and 10 in ref 22). In the nonpolar solvent, the gap is between 0 and 10 kcal/mol, depending on which C═C bond in the butadiene moiety is considered, whereas in the polar one it is 15−25 kcal/mol. Thus, the IC process is expected to be faster in the nonpolar solvent, though numerical values for the rate constants could not be extracted from the calculations. It should be borne in mind that the surface crossing can be very rapid even around an avoided crossing with a gap of 25 kcal/mol. The rates extracted from the femtosecond experiment, corroborated nicely by emission QY measurements as well, are about a factor of 2.5 larger in toluene. As this second step, associated with species B*, is assigned by our interpretation to the lifetime of $S_1$ (ZW) state, these factors are in line with the qualitative theoretical predictions.

Finally, $A_H$ is assigned to a vibrationally excited ground state ("hot" GS) after the $S_1$−$S_0$ crossing, and the time constant associated with it to a vibrational cooling process (step 3). This is supported by a near match between the spectra associated with this process in both samples, and a broadened first derivative of the ground state absorption spectra displayed in Figure 2 (see panel B of Figure S2 in the Supporting Information). The ∼5 ps time constant associated with this step, and its relative insensitivity to the change in solvent, are fully consistent with this assignment.

Another funnel, *cis*−*trans* isomerization around the middle bond, b5 (see Figure 1), as investigated by Burda et al.,[32] is not considered, as it can occur only if protonation takes place as discussed by Steiner et al.;[45] this process is not possible when aprotic, dry solvents are used, as in the present experiments. In a recent paper, Petkova et al. studied the ultrafast dynamics of several Green Fluorescence Protein derivatives in polar and nonpolar solvents.[46] Their work bears some similarity to ours, especially as far as nonprotic solvents were used. They also used a three-step mechanism to explain their data, and suggest for the second step a "large amplitude motion" that leads to the ground state. The nature of this motion was not specified, the yet most likely candidate being the torsion around the exocyclic C═C bond. We believe that a conical intersection is involved also in their systems 3 and 5, but no theoretical basis was given in the paper.

## E. CONCLUDING REMARKS

The effect of the solvent on the gap between the $S_1$ and $S_0$ states as a function of solvent polarity was discussed in a previous theoretical paper.[22] It was concluded that in nonpolar solvents the gap is smaller than in polar ones, so that the internal conversion process is expected to be faster in the nonpolar solvents. Therefore, the lifetime of the excited state should be shorter in nonpolar solvents. No quantitative data of these lifetimes are yet available from the computations, but as the estimated time scale for these processes is subpicosecond, ultrafast pump−probe technique is optimal for probing this time scale. Following our analysis, the excited state ultrafast signals are well-fit by a biexponential behavior, with a <100 fs component accounting for very fast dynamics (step 1) and a second exponent which can be assigned with high certainty to the excited state lifetime (step 2). Fitting of the data shows that the lifetime of the excited state is about 300−400 fs in toluene and 900−1000 fs in MeCN, in agreement with the trend predicted by theoretical predictions. This constitutes a demonstration of the possibility to tune the properties of a conical intersection by changing the solvent, which in turn was shown to be equivalent to applying an external electric field. Because electric fields can be continuously tuned, a continuous tuning of the CI may be experimentally feasible.

## ■ ASSOCIATED CONTENT

**Supporting Information.** Calculated vibrational modes of the di-tBu-MRCN in both solvents (Table S1), steady state absorption spectra analysis and calculation (Table S2, Figure S1, and text), and further information on the SADS steps assignment. This material is available free of charge via the Internet at http://pubs.acs.org.

## ■ AUTHOR INFORMATION

### Corresponding Author

*E-mail: yehuda@chem.ch.huji.ac.il (Y.H.); sandy@fh.huji.ac.il (S.R.).

### Author Contributions

†These authors contributed equally to the paper.

## ■ ACKNOWLEDGMENT

This work was supported by the Israel Science Foundation (ISF) which is administered by the Israel Academy of Sciences and Humanities (for A.W. and S.R.). A.K. thanks the Ministry of Science and Technology, for a Levi Eshkol Ph.D. Scholarship. A.W. is supported by the Adams Fellowship Program of the Israel Academy of Sciences and Humanities. The Minerva Farkas Center for Light Induced Processes is supported by the Minerva Gesellschaft GmbH, Munich, Germany.

## ■ REFERENCES

(1) Domcke, W.; Yarkony, D. R.; Köppel, H. *Conical Intersections: Electronic Structure, Dynamics and Spectroscopy*; World Scientific Publishing Co.: Singapore, 2004.
(2) Longuet-Higgins, H. C. *Proc. R. Soc., A.* **1975**, *344*, 147–156.
(3) Yarkony, D. *Rev. Mod. Phys.* **1996**, *68*, 985–1013.
(4) Zilberg, S.; Haas, Y. *Adv. Chem. Phys.* **2002**, *124*, 433–504.
(5) Brooker, L. G. S.; Keyes, G. H.; Sprague, R . H.; van Dyke, H.; van Lare, E.; Van Zandt, G.; White, F. L.; Cressman, H . W. J.; Dent, S. G., Jr. *J. Am. Chem. Soc.* **1951**, *73*, 5332–5350.
(6) Klessinger, M.; Michl, J. *Excited States and Photochemistry of Organic Molecules*; VCH Publishers: New York, Weinheim, 1995.
(7) Fuß, W.; Lochbrunner, S.; Müller, A. M.; Schikarski, T.; Schmid, W. E.; Trushin, S. A. *Chem. Phys.* **1998**, *232*, 161–174.
(8) Levine, B. G.; Martínez, T. J. *Annu. Rev. Phys. Chem.* **2007**, *58*, 613–634.
(9) Polli, D.; Altoe, P.; Weingart, O.; Spillane, K. M.; Manzoni, C.; Brida, D.; Tomasello, G.; Orlandi, G.; Kukura, P.; Mathies, R. A.; Garavelli, M.; Cerullo, G. *Nature* **2010**, *467*, 440–443.
(10) Farrow, D. A.; Qian, W.; Smith, E. R.; Ferro, A. A.; Jonas, D. M. *J. Chem. Phys.* **2008**, *128*, 144510.
(11) Olivucci, M.; Santoro, F. *Angew. Chem., Int. Ed.* **2008**, *47*, 6322–6325.

(12) Deckert, V.; Iwata, K.; Hamaguchi, H. *J. Photochem. Photobiol., A* **1996**, *102*, 35–38.
(13) (a) Burghardt, I.; Hynes, J. T. *J. Phys. Chem. A* **2006**, *110*, 11411–11423. (b) Burghardt, I.; Cederbaum, L. S.; Hynes, J. T. *Faraday Discuss.* **2004**, *127*, 395–411.
(14) Alfalah, S.; Deeb, O.; Zilberg, S.; Haas, Y. *Chem. Phys. Lett.* **2008**, *459*, 100–104.
(15) Squillacote, M.; Wang, J. S.; Chen, J. W. *J. Am. Chem. Soc.* **2004**, *126*, 1940–1941.
(16) Sussman, B. J.; Townsend, D.; Ivanov, M. Y.; Stolow, A. *Science* **2006**, *314*, 278–281.
(17) (a) Mitrić, R.; Hartmann, M.; Pittner, J.; Bonačić-Koutecký, V. *J. Phys. Chem. A* **2002**, *106*, 10477–10481. (b) Sukharev, M.; Seideman, T. *Phys. Rev. A: At., Mol., Opt. Phys.* **2005**, *71*, 012509. (c) Abe, M.; Ohtsuki, Y.; Fujimura, Y.; Lan, Z. G.; Domcke, W. *J. Chem. Phys.* **2006**, *124*, 224316. (d) Rozgonyi, T.; González, L. *Chem. Phys. Lett.* **2008**, *459*, 39–43.
(18) Lim, J. S.; Lee, Y. S.; Kim, S. K. *Angew. Chem., Int. Ed.* **2008**, *47*, 1853–1856.
(19) (a) Gustavsson, T.; Sarkar, N.; Lazzarotto, E.; Markovitsi, D.; Barone, V.; Improta, R. *J. Phys. Chem. B* **2006**, *110*, 12843–12847. (b) Gustavsson, T.; Sarkar, N.; Lazzarotto, E.; Markovitsi, D.; Improta, R. *Chem. Phys. Lett.* **2006**, *429*, 551–557. (c) Santoro, F.; Barone, V.; Gustavsson, T.; Improta, R. *J. Am. Chem. Soc.* **2006**, *128*, 16312–16322.
(20) Briand, J.; Bram, O.; Rehault, J.; Leonard, J.; Cannizzo, A.; Chergui, M.; Zanirato, V.; Olivucci, M.; Helbing, J.; Haacke, S. *Phys. Chem. Chem. Phys.* **2010**, *12*, 3178–3187.
(21) (a) Arasaki, Y; Takatsuka, K. *Phys. Chem. Chem. Phys.* **2010**, *12*, 1239–1242. (b) Arasaki, Y.; Wang, K. H.; McKoy, V.; Takatsuka, K. *Phys. Chem. Chem. Phys.* **2011**, *13*, 8681–8689.
(22) Xu, X. F.; Kahan, A.; Zilberg, S.; Haas, Y. *J. Phys. Chem. A* **2009**, *113*, 9779–9791.
(23) da Silva, L.; Machad, C.; Rezende, M. C. *J. Chem. Soc., Perkin Trans. 2* **1995**, *2*, 483–488.
(24) Mishra, A.; Behera, R. K.; Behera, P. K.; Mishra, B. K.; Behera, G. B. *Chem. Rev.* **2000**, *100*, 1973–2011.
(25) Brooker, L. G. S.; Craig, A. C.; Heseltin, D. W.; Jenkins, P. W.; Lincoln, L. L. *J. Am. Chem. Soc.* **1965**, *87*, 2443–2450.
(26) Würthner, F.; Archetti, G.; Schmidt, R.; Kuball, H. -G. *Angew. Chem., Int. Ed.* **2008**, *47*, 4529–4532.
(27) Kovalenko, S. A.; Ernsting, N. P.; Ruthmann, J. *Chem. Phys. Lett.* **1996**, *258*, 445–454.
(28) Maciejewski, A.; Naskrecki, R.; Lorenc, M.; Ziolek, M.; Karolczak, J.; Kubicki, J.; Matysiak, M.; Szymanski, M. *J. Mol. Struct.* **2000**, *555*, 1–13.
(29) Martin, M. M.; Plaza, P.; Meyer, Y. H. *Chem. Phys.* **1995**, *192*, 367–377.
(30) Minch, M. J.; Shah, S. S. *J. Chem. Educ.* **1977**, *54*, 709.
(31) Gruda, I.; Bolduc, F. *J. Org. Chem.* **1984**, *49*, 3300–3305.
(32) Burda, C.; Abdel-Kader, M. H.; Link, S.; El-Sayed, M. A. *J. Am. Chem. Soc.* **2000**, *122*, 6720–6726.
(33) Rurack, K.; Spieles, M. *Anal. Chem.* **2011**, *83*, 1232–1242.
(34) Bismuth, O.; Komm, P.; Friedman, N.; Eliash, T.; Sheves, M.; Ruhman, S. *J. Phys. Chem. B.* **2010**, *114*, 3046–3051.
(35) Strickler, S. J.; Berg, R. A. *J. Chem. Phys.* **1962**, *37*, 814–822.
(36) (a) Henry, E. R.; Hofrichter, J. *J. Methods Enzymol.* **1992**, *210*, 129–192. (b) van Stokkum, I. H. M.; Larsen, D. S.; van Grondelle, R. *Biochim. Biophys. Acta, Bioenerg.* **2004**, *1657*, 82–104.
(37) Catalan, J.; Mena, E.; Meutermans, W.; Elguero, J. *J. Phys. Chem.* **1992**, *96*, 3615–3621.
(38) Morley, J. O.; Morley, R. M.; Fitton, A. L. *J. Am. Chem. Soc.* **1998**, *120*, 11479–11488.
(39) Murugan, N. A.; Kongsted, J.; Rinkevicius, Z.; Agren, H. *Phys. Chem. Chem. Phys.* **2011**, *13*, 1290–1292.
(40) Mustroph, H.; Mistol, J.; Senns, B.; Keil, D.; Findeisen, M.; Hennig, L. *Angew. Chem., Int. Ed.* **2009**, *48*, 8773–8775.
(41) (a) Heller, E. J. *Acc. Chem. Res.* **1981**, *14*, 368–375. (b) Tannor, D. J.; Heller, E. J. *J. Chem. Phys.* **1982**, *77*, 202–218. (c) Myers, A. B. *J. Raman. Spectrosc.* **1997**, *28*, 389–401.
(42) Mach, P.; Urban, J.; Leszcynski, J. *Int. J. Quantum Chem.* **2002**, *87*, 265–269.
(43) Baraldi, I.; Brancolini, G.; Momicchioli, F.; Ponterini, G.; Vanossi, D. *Chem. Phys.* **2003**, *288*, 309–325.
(44) Murugan, N. A.; Kongsted, J.; Rinkevicius, Z.; Aidas, K.; Ågren, H. *J. Phys. Chem. B* **2010**, *114*, 13349–13357.
(45) Steiner, U.; Abdel-Kader, M. H.; Fischer, P.; Kramer, H. E. A. *J. Am. Chem. Soc.* **1978**, *100*, 3190–3197.
(46) Petkova, I.; Dobrikov, G.; Banerji, N.; Duvanel, G.; Perez, R.; Dimitrov, V.; Nikolov, P.; Vauthey, E. *J. Phys. Chem. A* **2009**, *114*, 10–20.